Invited Paper

Surface Energy Effects on the Self-Assembly of Epitaxial Quantum Dots

Lawrence H. Friedman

Penn State University, 212 Earth and Engineering Sciences Building, University Park, PA 16802

ABSTRACT

Epitaxial self-assembled quantum dots (SAQDs) result from Stranski-Krastanow growth whereby epitaxial 3D islands form spontaneously on a planar thin film. Common systems are Ge_xSi_{1-x}/Si and $In_xGa_{1-x}As/GaAs$. SAQDs are typically grown on a (001) surface. The formation and evolution of SAQDs is governed in large part by the interaction of surface energy and elastic strain; however, the surface energy density is quite complicated and not well understood. Many growth processes take place at high temperature where stress and entropy effects can have a profound effect on the surface free energy. There are three competing theories of the nature of the planar (001) surface: I. It is a stable crystal facet. II. It is a stable non-faceted surface. III. It is an unstable crystal antifacet. Each leads to a different theory of the SAQD formation process. The first theory appears most often in modeling literature, but the second two theories take explicit account of the discrete nature of a crystal surface. Existing observational and theoretical evidence in support of and against these theories is reviewed. Then a simple statistical mechanics model is presented that yields a phase-diagram depicting when each of the three theories is valid. Finally, the Solid-on-Solid model of crystal surfaces is used to validate the proposed phase diagram and to calculate the orientation and height dependence of the surface free energy that is expressed as a wetting chemical potential, a wetting modulus and surface tilt moduli.

Keywords: quantum dots, self-assembly, epitaxial growth, surface energy, roughening, SOS model, step-edges, films, GeSi, InGaAs

1. INTRODUCTION

Production of reliable and high quality heteroepitaxial self-assembled quantum dots (SAQDs) will represent an important step in the advancement of semiconductor fabrication at the nanoscale allowing breakthroughs in optoelectronics and electronics.[1–11] SAQDs are the result of a transition from 2D growth to 3D growth in strained epitaxial films such as Si_xGe_{1-x}/Si and $In_xGa_{1-x}As$/GaAs. This process is known as Stranski-Krastanow growth.[3,12–14] For SAQDs to compete with traditional lithography, they must be designable or at least reproducible. The design of SAQD fabrication processes will rely on computational modeling, but even today, there are still outstanding fundamental questions regarding how to model SAQD formation. There are essentially three competing models of SAQD growth: I. the nucleation and growth model,[15] II. the surface linear instability model,[16–18] also known as the Asarro-Tiller-Grinfeld (ATG) instability model, and III. the surface non-linear instability model.[19] These three models correspond to three states of the crystal (001) surface: I. a faceted surface with positive step-edge energy, II. a thermally roughened surface, and III. an anti-faceted surface with negative step-edge energy. The distinctions between these three models and the corresponding states of the crystal surface require clarification. For Ge_xSi_{1-x}/Si SAQDs, the same experimental evidence[20–22] has been cited as supporting either model II[22] or III,[23] and it is only recently that the ATG model (II) has been applied to $In_xGa_{1-x}As$/GaAs.[24,25] Here, the evidence in support of the three SAQD formation models is discussed, and a simplified statistical mechanics model of the strained stepped crystal surface is reported that helps to resolve the existing ambiguities and clarify the role of crystal surface energy in determining SAQD formation and morphology. In addition, the solid-on-solid (SOS) model is used to demonstrate calculations of wetting energies and isotropic and anisotropic surface tilt-moduli. The presented models have many simplifying approximations, but they clarify the ambiguity in SAQD growth processes, thereby bringing reliable models usable for design and optimization of fabrication processes a step closer.

Further author information: (Send correspondence to L.H.F.)
E-mail: lfriedman@psu.edu, Telephone: 1 814 865 7684

Quantum Dots, Particles, and Nanoclusters VI,
edited by Kurt G. Eyink, Frank Szmulowicz, Diana L. Huffaker, Proc. of SPIE Vol. 7224,
722405 · © 2009 SPIE · CCC code: 0277-786X/09/$18 · doi: 10.1117/12.809796

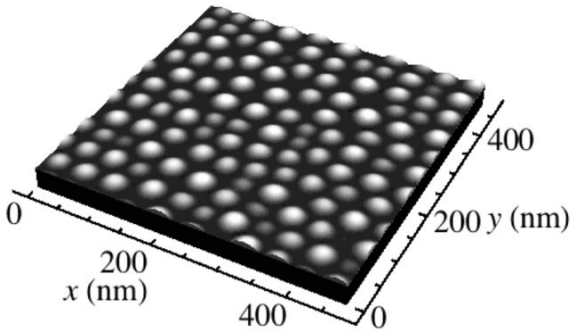

Figure 1. Snapshot of a continuum simulation of Ge/Si SAQD formation similar to Ref.[25] Dots have a lens or mound shape because all surface energy anisotropy is neglected.

1.1 The crystal surface energy

In strained film or SAQD growth models, the crystal surface or film height evolves in a fashion that dissipates free energy. The dependent variable, $\overline{h}$, is a continuous order parameter that is a function of $\mathbf{x}$, the vector position in the $x-y-$plane, usually the (001) plane. $\overline{h}(\mathbf{x})$ is indicative of the film height but not identically equal to it. In contrast, the actual film height takes on discrete values at the atomic scale $h(\mathbf{x}) = H(\mathbf{x})\, h_0$, where $H(\mathbf{x})$ is an integer. In Sec. 3, $\overline{h}(\mathbf{x})$ is set to be an ensemble average of atomic-scale film heights $\overline{h} = \langle h \rangle$. In many instances, the details of how $\overline{h}(\mathbf{x})$ relates to $h(\mathbf{x})$ are ignored, and one simply writes down a phenomenological evolution equation, for example, $\partial_t \overline{h}(\mathbf{x},t) = \nabla \cdot \tilde{D} \cdot \nabla[\delta f[\overline{h}]/\delta \overline{h}(\mathbf{x})]$, where $f[\overline{h}]$ is the free energy and $\tilde{D}$ is the diffusivity. A snapshot of such a simulation is shown in Fig. 1. It is also possible to add other terms such as condensation terms,[26] random deposition terms[25] or stochastic thermal fluctuations in surface diffusion.[25,27]

The film free energy $f[\overline{h}]$ is sum that includes the elastic strain energy, f_e, that tends to destabilize 2D film growth, and the surface and wetting energy, f_{sw}; thus, $f = f_e + f_{sw}$. Often, the second contribution is broken in up into the sum of two terms, $f_{sw} = f_s + f_w$, where f_s is the surface free energy and f_w is the wetting energy, but it is unclear whether such a deconvolution is accurate. The details of f_{sw} greatly influence both small-scale morphology such as shape[22,28] and large-scale morphology such as quasiperiodicity and order.[24,27] It is most often assumed that the surface and wetting energy f_{sw} is an integral over a local energy density that is a local function of the film height ($\overline{h}(\mathbf{x})$) and gradient ($\nabla \overline{h}(\mathbf{x})$) so that

$$f_{sw} = \int d^2\mathbf{x}\, w\left[\overline{h}(\mathbf{x}), \nabla \overline{h}(\mathbf{x})\right].$$

The three cases of the crystal surface free energy map onto two forms of the kernel w.[23,29]

case I. Facet If a faceted film surface has an (001) orientation, the energy density is believed to be a local function of the gradient magnitude,[29]

$$w = w_w\left(\overline{h}\right) + \gamma_1 \left|\nabla \overline{h}(\mathbf{x})\right| + \gamma_3 \left|\nabla h(\mathbf{x})\right|^3 + \ldots, \tag{1}$$

where $w_w\left(\overline{h}\right) = w\left(\overline{h}, \nabla \overline{h} = \mathbf{0}\right)$ is the wetting energy density. In the anisotropic case with steps in two orthogonal directions, e.g. x and y,

$$w = w_w\left(\overline{h}\right) + \gamma_x \left|\partial_x \overline{h}(\mathbf{x})\right| + \gamma_y \left|\partial_x \overline{h}(\mathbf{x})\right| + \gamma_{xxx} \left|\partial_x \overline{h}(\mathbf{x})\right|^3 + \ldots. \tag{2}$$

The first order term is the step-edge energy per unit length, $e_{x(y)}/a_s$, times step edge density, $\left|\partial_x \overline{h}(\mathbf{x})/h_0\right|$; $\gamma_{x(y)} = e_{x(y)}/(h_0 a_s)$. Higher order terms include step-step interactions.

case II. Thermally roughened. Above the roughening transition temperature, T_R, the (001) facet thermally roughens, and the leading gradient dependent term in the surface energy kernel is quadratic in $\nabla \overline{h}(\mathbf{x})$,[29]

$$w = w_w\left(\overline{h}\right) + \frac{1}{2}\tilde{w}^{(0,2)} : \left[\nabla \overline{h}(\mathbf{x}) \otimes \nabla \overline{h}(\mathbf{x})\right] + \ldots, \tag{3}$$

where $\tilde{w}^{(0,2)}$ is the second derivative of $w\left[\overline{h},\nabla\overline{h}\right]$ with respect to $\nabla\overline{h}$.

case III. Antifacet. It was hypothesized and demonstrated using atomic-scale empirical potential models that under intense surface strain, the step-edge energy can actually become negative.[23] In this case, the free energy kernel is the same as in case I (Eqs. 1 and 2), but $\gamma_{x(y)}$ is negative.

The form of the free energy density (w) determines how easily a surface can be perturbed from being flat by a destabilizing force density. Assuming that w is a function of $\overline{h}$ and $\nabla\overline{h}$, one can define three important quantities for a flat film of height $\overline{h}$: the wetting chemical potential $m_w = \partial w/\partial\overline{h}$, the wetting modulus, $w^{(2,0)} = \partial^2 w/\partial\overline{h}^2$ and the tilt modulus, $\tilde{w}^{(0,2)} = \partial^2 w/\partial\nabla\overline{h}^2$. The tilt modulus includes the effects of increased surface area as the surface tilts as well as the change in the energy density, $\gamma\left(\nabla\overline{h}\right)$; $\tilde{w}^{(0,2)} = \left[\gamma\left(\nabla\overline{h}\right)\tilde{I} + \partial^2_{\nabla\overline{h}}\gamma\left(\nabla\overline{h}\right)\right|_{\nabla\overline{h}=\mathbf{0}}$. In pattern formation problems such as epitaxial SAQD formation, it is often useful to know how the energy changes when a sinusoidal perturbation is introduced.[30–32] Writing a Fourier series for the film height, $\overline{h}(\mathbf{x}) = \sum_{\mathbf{k}} e^{i\mathbf{k}\cdot\mathbf{x}}\overline{h}_{\mathbf{k}}$, and $\overline{h}_{\mathbf{k}} = A^{-1}\int d^2\mathbf{x}\, e^{-i\mathbf{k}\cdot\mathbf{x}}\overline{h}(\mathbf{x})$, where A is the film surface area projected onto the $x-y-$plane, and $\overline{h}_{-\mathbf{k}} = \overline{h}^*_{\mathbf{k}}$ so that $\overline{h}(\mathbf{x})$ is real. Assuming that $\overline{h}_{\mathbf{k}}$ is small whenever $\mathbf{k}\neq\mathbf{0}$, and noting that $\overline{h}_{\mathbf{0}}$ is the spatially averaged film height, one can write down the free energy in terms of the Fourier components,

$$f_{sw} = Aw_w\left(\overline{h}_{\mathbf{0}}\right) + \frac{A}{2}\sum_{\mathbf{k}\neq\mathbf{0}} w^{(2)}_{\mathbf{k},-\mathbf{k}}\left|\overline{h}_{\mathbf{k}}\right|^2 + \ldots, \tag{4}$$

where

$$w^{(2)}_{\mathbf{k}_1,\mathbf{k}_2} = \frac{\partial^2\left(f_{sw}/A\right)}{\partial\overline{h}_{\mathbf{k}_2}\partial\overline{h}_{\mathbf{k}_1}} = \left(w^{(2,0)} + \mathbf{k}_1\cdot\tilde{w}^{(0,2)}\cdot\mathbf{k}_1\right)\delta_{\mathbf{k}_1+\mathbf{k}_2} \tag{5}$$

can be considered the surface modulus in Fourier space, and $\delta_{\mathbf{k}_1+\mathbf{k}_2}$ is the Kronecker Delta that is equal to 1 when $\mathbf{k}_1 = -\mathbf{k}_2$ and equals 0 otherwise. The Fourier components of the chemical potential are

$$m_{\mathbf{k}} = \frac{\partial\left(f_{sw}/A\right)}{\partial\overline{h}_{-\mathbf{k}}} = \left[w^{(1)}_w\left(\overline{h}_{\mathbf{0}}\right) - w^{(2,0)}\overline{h}_{\mathbf{0}}\right]\delta_{\mathbf{k}-\mathbf{0}} + w_{\mathbf{k},-\mathbf{k}}\overline{h}_{\mathbf{k}} \tag{6}$$

If the rank-2 tensor, $\tilde{w}^{(0,2)}$ has eigenvectors in the $x-$ and $y-$directions with eigenvalues $w^{(0,2)}_x$ and $w^{(0,2)}_y$, then

$$w^{(2)}_{\mathbf{k},-\mathbf{k}} = w^{(2,0)} + w^{(0,2)}_x k_x^2 + w^{(0,2)}_y k_y^2. \tag{7}$$

As can be seen from Eqs. 4, the larger the surface modulus, the more energy it costs to perturb the flat surface. The wetting modulus tends to stabilize a flat surface against all perturbations, while the tilt modulus tends to stabilize against high wave vector (short wavelength) perturbations.

The three discussed cases can be distinguished by the nature of their tilt modulis. In case I. faceting, the tilt moduli are essentially infinite and positive, so that it is impossible to perturb the surface with a small force. For case II. roughened surface, the tilt moduli are positive and finite, so that the surface is perturbable, and for case III. antifaceting, the tilt moduli are negative and infinite so that there is a large internal force that roughens the surface even in the absence of other effects. Due to these differences in the resistance of the film surface to perturbation, three very different models of SAQD formation result. They are as follows:

case I. Nucleation and Growth (faceting) The flat film is extremely stable with an infinite surface modulus, but it is possible to form localized structures whose faces are also facets such as in the $\{105\}$ directions.[15] Thus, SAQDs form that are highly shape-constrained and have a total free energy f as a function of volume $f(V) = aV^{2/3} - bV$, where a is the rate of energy cost due to the increased crystal surface, and b is the energy released due to elastic strain relief. The free energy peaks when $V^* = [a/(3b)]^3$. Plugging into f, the SAQDs form with an energy barrier of $f(V^*) = (4/27)a^3/b^2$. This model treats SAQD formation as a localized nucleation and growth event.

case II. Linear instability (roughening) In this case, the flat film surface is perturbable, and one sees a more cooperative SAQD formation process where quasiperiodic arrays of SAQDs form essentially simultaneously. In this case, it is guaranteed that there will be some circumstances for which a 2D film is unstable. For large film heights, the substrate

would be less important so that the wetting modulus goes to zero ($w^{(1,0)} \to 0$). The surface modulus (Eq. 5) should decrease even further when one considers very large wavelengths (small $\mathbf{k}$). Thus, for sufficiently large film heights, there is some wavelength long enough that the flat film surface can be easily perturbed. In the ATG model,[16–18,33,34] the perturbing force is a self-excitation, where the amount of released elastic free energy is proportional to the magnitude of the wave vector, $\|\mathbf{k}\|$. Using the elastic energy release coefficients, combined with the surface and wetting moduli, one can find a critical film height for the transition from 2D to 3D growth, the mean perturbation wavelength and the orientation of SAQD arrays.

case III. Nonlinear instability (antifaceting) In this case, no additional perturbation is required.[35] The flat film is at an infinitely sharp free energy maximum and finds a suitable faceting direction that is a free energy minimum. For Ge_xSi_{1-x}/Si, this is the (105) orientation. In this case, the elastic strain energy is almost irrelevant to the initial formation, and its role is to drive coarsening once SAQDs have initially formed. At smaller scales, coarsening takes place via dot coalescence. Once dots reach a certain size, coarsening takes place by competition for material with larger dots siphoning material from smaller dots.

1.2 Reconciling the three models.

The discussion of these three models now begs the question, which is correct? Is it more than one with different mechanisms occurring under different circumstances? This question has been studied most with regard to Ge_xSi_{1-x}/Si SAQDs, but patterns of In_xGa_{1-x}As/GaAs dots also contribute some evidence to the discussion. Although, at this point it is hard to have a conclusive answer, most observations seem to be explained be explained by the ATG model with the least amount of theoretical discomfort. First, some experimental evidence is considered, and then the theoretical arguments.

1.2.1 Experimental Evidence

First, consider Ge_xSi_{1-x}/Si experiments. Although, the faceting model or nucleation and growth model (I) was originally developed to describe Ge_xSi_{1-x}/Si SAQD dot formation, it appears to have more staying power applied to In_xGa_{1-x}As/GaAs dots. In particular, key experimental observations[20–22] suggest that the nucleation and growth model does not apply to Ge_xSi_{1-x}/Si SAQDs. According to the nucleation and growth model, SAQDs should start off as small faceted dots and grow in a self-similar manner with an occasional shape-transformation once certain critical volumes are achieved. In Refs.,[20–22] it was observed that SAQDs appear to form as low-aspect ratio surface perturbations that grow vertically into fully formed SAQDs. Tersoff, *et al.*[22] claimed that these observations support Model II, that the strained (001) Ge_xSi_{1-x} surface is stable, but not a facet, *i.e.* it has a finite resistance to small perturbations, not an infinite one. Shenoy, *et al.*[23] and Ramasubramaniam and Shenoy[35] claim that this observation supports Model III, Antifaceting leading to a nonlinear surface instability.

It would appear, however, that the experimental evidence better supports Model II, the ATG model. It was observed that early in the formation of Ge_xSi_{1-x}/Si SAQDs, a recognizable characteristic wavelength develops and persists as growth continues.[20] Growth occurring at a characteristic wavelength is typical of linear instability models and is certainly predicted by the ATG model. The Antifaceting model (III) should result in many initially small dots with (105) facets that coalesce into larger dots. Thus, there should be an initially small characteristic wavelength that grows longer during coarsening, in contradiction to the experimental observations. In favor of the antifaceting model over the ATG model, it was pointed out that the ATG model predicts roll-like structures where individual dots have material bridges during the initial stages of growth, whereas such structures are not observed experimentally. This evidence, however, is ambiguous as it is unclear how long the bridges should persist. In Ref.,[25] such bridges only lasted for atomic-scale fluctuations. Atomic scale variations in an order parameter would manifest as a local bias of film roughness that would be difficult to observe.

Some In_xGa_{1-x}As/GaAs structures also exhibit characteristic length scales reminiscent of the cooperative ATG process. At high temperatures one can find rolls (Figs. 2c and d in Ref.[36]), correlated dense arrays of SAQDs (Fig. 1 in Ref.[37]) and quantum dot chains in multilayers (Fig. 1a in Ref.[38]). Such patterns at high temperature suggest that the surface has been thermally roughened, resulting in an ATG-like process.[24]

1.2.2 Theoretical Evidence

The theoretical evidence appears at first to support models I and III, but further analysis suggests that Model II might be the most applicable model. Models I and III, based respectively on faceting and antifaceting of the (001) surface, are persuasive

in that they take explicit account of atomic-scale crystal step edges . Furthermore, in favor of the anti-faceting model (III), the necessary reduction in step-edge energy with increasing compressive strain was calculated through atomistic empirical potential calculations.[19] However, Model III omits the effects of configurational entropy. It is essentially a zero-Kelvin model that considers total energies of non-fluctuating crystal morphologies instead of free energies of fluctuating ones. At finite temperature, the free energy of a fluctuating step edge is $f = \langle u \rangle - k_b T s$, where $\langle u \rangle$ is the mean total energy, k_b is Boltzmann's constant, and s is the entropy. The roughening transition occurs when the step free energy goes to zero so that steps spontaneously form.[39,40] It is impossible that the mean energy $\langle u \rangle$ of a step becomes negative before the step free energy. Thus, if the antifaceting model (III) applies at all, there must also be some conditions under which the ATG model (II) applies. Furthermore, once one considers entropy effects, it is clear that even when $\langle u \rangle$ becomes zero or less that the maximum entropy state is a statistically flat surface. If the film surface is everywhere a $\{105\}$ orientation, it will maximize entropy by randomly switching between segments that are (105) and $(\bar{1}05)$, etc. Such random switching leads to a surface that is flat in the mean with $\langle h(\mathbf{x}) \rangle = \text{constant}$, but with a significant amount of fluctuation, $\left\langle h(\mathbf{x})^2 \right\rangle > 0$. This effect is similar to the entropic spring model of polymer stretching, and this state of the crystal surface is essentially a roughened surface (model II). A Solid-On-Solid statistical mechanics models of surfaces with some positive and some negative step energies would tend to support this second view.[41] Thus, it seems likely that strain effects lower the roughening temperature of strained film surfaces, but they do not lead to an anti-faceting SAQD growth model.

2. SIMPLE MODEL OF GROWTH REGIMES

It is possible to construct a phase diagram that indicates when each of the three proposed SAQD growth models applies by using a simple step-edge energy model based on the rule of mixtures combined with the step-edge strain sensitivity modeled by Shenoy *et. al*[23] and the step-edge free energy model proposed by Zandvliet.[39,40] In Ge and Si, it was observed that monolayer S_A and S_B step-edges have fluctuating kinks that have lengths equal to the diagonal length of a unit cell, $a_S = \sqrt{2}a_0 = 7.68\,\text{Å}$, and that are separated by the same amount, a_S (Figs. 1 and 2 in Ref.[40] and Fig. 2 in Ref.[39]). These kinks are thermal excitations of a straight step-edge, and the free energy of a fluctuating step-edge can be estimated using the step-edge energy $e_{S_A(S_B)}$ and the second-nearest neighbor interaction energy, e_{SNN}.

The step-edge free energy for each length a_s is approximately[39,40]

$$f_{S_A(S_B)} \approx e_{S_A(S_B)} - k_b T \ln\left(1 + \frac{2\exp\left[e_{SNN}/\left(k_b T\right)\right]}{\exp\left[e_{S_B(S_A)}/\left(k_b T\right)\right] - 1}\right), \tag{8}$$

The roughening transition occurs when $f^{S_A(S_B)} \to 0$, and the roughening temperature can be found numerically in terms of $e_{S_A(S_B)}$ and e_{SNN}. $f_{S_A(S_B)} \to 0$ at the same temperature for both kinds of steps. By analyzing STM micrographs of step edge kink densities, Zandvliet[39,40] was able to determine the step-edge and second nearest neighbor energies for unstrained Si and Ge (001) surfaces. For unstrained Si, $e_{S_A,\,\text{Si}} = 53 \pm 26$ meV, $e_{S_B,\,\text{Si}} = 124 \pm 27$ meV, and $e_{SNN,\,\text{Si}} = -67 \pm 20$ meV.,[39] giving an estimated roughening temperature of $T_{R,\,\text{Si}} = 1342 \pm 108$ K in agreement with experimental observations of roughening at $T = 1483$ K. For unstrained Ge, $e_{S_A,\,\text{Ge}} = 102 \pm 7$ meV, $e_{S_B,\,\text{Ge}} = 41 \pm 7$ meV, and $e_{SNN,\,\text{Ge}} = 0 \pm 5$ meV.,[40] giving an estimated roughening temperature of $T_{R,\,\text{Ge}} = 887 \pm 115$ K, in agreement with an observed high temperature phase transition at $T = 955$ K.

When the alloy composition of $\text{Ge}_x\text{Si}_{1-x}/\text{Si}$ film changes from $x = 0$ to $x = 1$, two things happen. First, the step-edge energy changes due to chemical mixing. Second, as observed in the calculations by Shenoy, *el al.* ,[19] the step-edge energy decreases as the biaxial strain becomes more compressive. A simple model of the strain-sensitivity can be used to demonstrate the effect on the step-edge energies and free energies. In atomistic calculations, the strain sensitivity varied greatly depending on which empirical potentials were used, so for simplicity, it is assumed here that all three step-edge energies can be characterized by a single strain-sensitivity (α) that will be chosen *ad hoc* to conform best with experimental observation. Thus, the form for the step-edge energy is

$$e_i(x) = \left[e_{i,\,\text{Si}}(1-x) + e_{i,\,\text{Ge}}(x)\right](1 + \alpha\varepsilon_0 x), \tag{9}$$

where $i = S_A$, S_B or SNN, and $\varepsilon_0 = -0.04$ is the biaxial strain in a Ge/Si film. With lower step-edge energies, the roughening temperature should be lower as well.

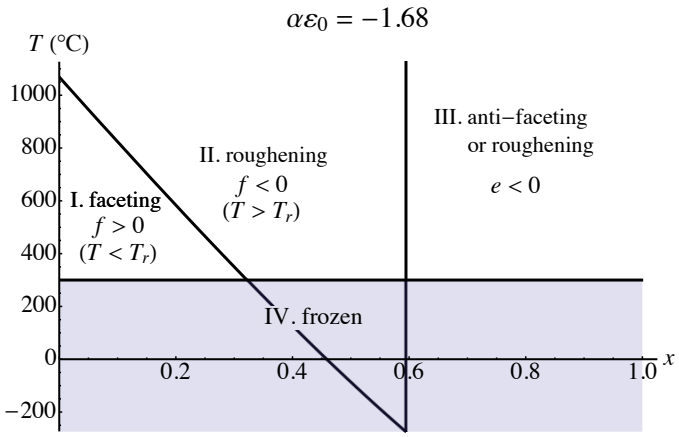

Figure 2. Ge_xSi_{1-x}/Si (001) surface phase diagram corresponding to $\alpha\varepsilon_0 = -1.68$ as calculated using Eqs. 8 and 9. Four phases or SAQD growth regimes are found.

Plugging the strain-dependent step-edge energy, Eq. 9 into the step-edge free energy formula (Eq. 8), one obtains a phase diagram for the strained film surface. Fig. 2 shows the phase diagram corresponding to $\alpha = 42$ or $\alpha\varepsilon_0 = -1.68$. There are four regions or phases:

I. Faceted $f_{S_A(S_B)} > 0$, and $e_{S_A(S_B)} > 0$ so that the (001) surface is a crystal facet. SAQD formation should follow growth model I that requires thermal activation and SAQD nucleation should be somewhat rare.[15]

II. Roughened $f_{S_A(S_B)} < 0$, and $e_{S_A(S_B)} > 0$. The (001) crystal surface is roughened. SAQD formation should take place via growth model II, the ATG mechanism starting first with the formation of organized surface ripples.

III. Anti-faceted or roughened $f_{S_A(S_B)} < 0$, and $e_{S_A(S_B)} < 0$. Both the step-edge free energy and total energy are negative. As discussed in Sec. 1.2.2, it is unclear whether the surface acts as an entropic spring in which case SAQD growth model II applies, or whether it is best modeled as nonlinear instability as described in Ref.,[35] SAQD growth modell III.

IV. Frozen Region IV is not really a phase, but below the surface diffusion freeze-out temperature, the diffusion rate is so small that no significant surface evolution takes place, and the surface free energy is irrelevant. For Ge, this temperature is about $T_{FO} = 300 \pm 75$°C.

The presented step-edge free energy model and resulting diagram should be taken as approximate because it is based on guessed forms for the step-edge energies and strain sensitivities of Ge_xSi_{1-x}/Si film surfaces (Eq. 9); however, when $\alpha\varepsilon_0 = -1.68$ (Fig. 2), its predictions are consistent with observation of Ge_xSi_{1-x}/Si SAQD growth at $T = 670$°C[20] . It was observed that there was a minimum value of Ge content for which SAQDs form, $x_{\text{min.}} \approx 0.2$. In Fig. 2, the $x = 0.2$, $T = 670$°C point lies on the I-II phase boundary, suggesting that thermal activation of SAQD formation is rare, but upon roughening, SAQDs form via the ATG mechanism and are ubiquitous. A second transition was experimentally observed at $x = 0.6$, that lies on the II-III phase boundary in Fig. 2. For $x > 0.6$, dots were seen to be far less correlated. Perhaps this change in behavior is due to a different formation mechanism that might result if the ATG mechanism switches over to the antifaceting mechanism, or perhaps it is just related to a significant drop in the surface modulus. In the middle region, $0.2 < x < 0.6$, fairly prominent long characteristic wavelengths ($\sim 100 - 200$ nm) were observed (Fig. 3 in Ref.[20]), a phenomenon that is typical of the ATG formation mechanism. Thus, despite its gross approximations, the presented model appears to explain different observed growth regimes for an appropriate choice of the strain-sensitivity. The model does, however, have one more major shortcoming, while it predicts that surface strain lowers the roughening temperature, T_R, in Ge_xSi_{1-x}/Si films, it does not provide an estimate for the finite surface modulus ($w^{(2)}_{\mathbf{k},-\mathbf{k}}$) when $T > T_R$. To find the surface modulus one can use the more sophisticated, but also more cumbersome Solid-On-Solid (SOS) model.[41,42]

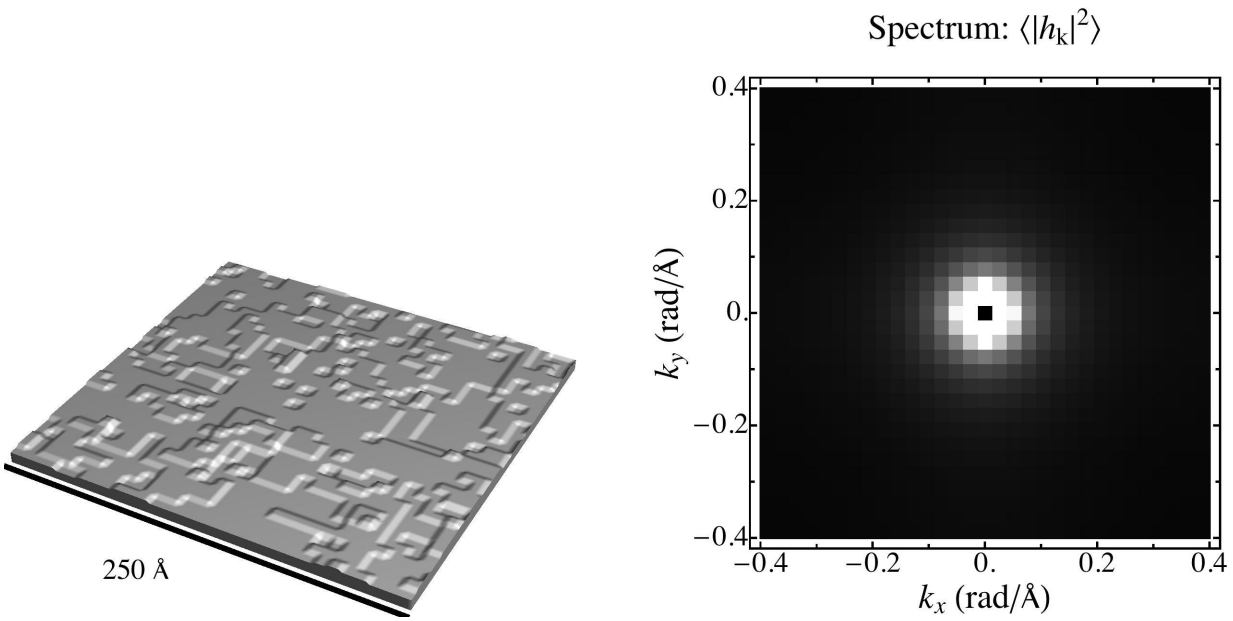

(a) (b)

Figure 3. Solid on Solid (SOS) model for $m_w = 6.29 \times 10^{-6}$ meV/Å^3 from Series 1 in Sec. 3.2.3. Fig. (a) shows a snapshot of fluctuating discrete film heights. Fig. (b) shows the time averaged spectrum $\langle |h_{\mathbf{k}}|^2 \rangle$ after about 200×10^6 steps.

3. SURFACE MODULUS AND THE SOS MODEL

The Solid-On-Solid (SOS) model is used to evaluate the surface modulus, $w^{(2)}_{\mathbf{k},-\mathbf{k}}$ (Fig. 3).[41,42] The SOS model gives both the wetting modulus ($w^{(2,0)}$) and the tilt modulus ($\tilde{w}^{(0,2)}$) as a function of the film height order parameter ($\overline{h}$) and temperature (T). In this model, film height (h) is a discrete variable on a lattice. Monolayer steps, kinks and islands arise naturally. Since the purpose here is to provide a proof of concept, the model is kept simple by assuming a square lattice with step-edges perpendicular to the $x-$ and $y-$ directions (Fig. 3). This structure is appropriate for one layer because of surface reconstruction and discrete step-edge lengths,[39] but layer-to-layer relationships appropriate for a diamond crystal structure are not properly maintained.[41] The square-lattice has spacing equivalent to the smallest kink size and spacing in Si, $a_s = 7.68$ Å.[39] Steps have a height h_0 and step-edge energies, e_x and e_y (Eq. 12).

Using this model, the following calculations are performed. First, it is demonstrated that the wetting potential arises naturally as an effect of configurational entropy using a simplification that neglects step-edge energies (Sec. 3.1). Then, Monte Carlo calculations of the SOS model are presented that include step-edge energies and estimate both the wetting and tilt moduli (Sec. 3.2). In these calculations, the SOS model is applied three cases: 1. a roughened ($T > T_R$) film with isotropic step-edge energies ($e_x = e_y$) and varying wetting chemical potential (m_w), 2. a faceted isotropic film ($T < T_R$), and 3. a roughened film with anisotropic step-edge energies ($e_x \neq e_y$). The last case is motivated by prior work on the influence of anisotropic tilt moduli on $In_xGa_{1-x}As$/GaAs film morphology.[24] Values of physical constants are given in Table 1. In general full calculations are performed using dimensionless quantities (capital letters), but results are reported here in dimensional quantities (lower-case letters).

3.1 Simple Wetting Model

A simple wetting model illustrates the entropic origins of the wetting potential or height dependence of the surface energy. A Lagrange multiplier m_w is introduced to control the mean film height $\langle h \rangle$. m_w is in fact the wetting chemical potential, $m_w = \delta f / \delta \overline{h}$. For absolute simplicity, step-edge energies are neglected $e_x = e_y = 0$. When new material is added, a bonding energy (e_b) is released. Thus, the energy as a function of the film height at a particular lattice site is $u(h) = -e_b(h/h_0)$,where $h = 0h_0, 1h_0, 2h_0, \ldots$. First the partition function at a lattice site is calculated,

$$Z(m_w) = \sum_{H=0}^{\infty} \exp\left[-\frac{1}{k_b T}\left(-e_b - m_w h_0 a_s^2\right) H\right] = 1/\left\{1 - \exp\left[\frac{1}{k_b T}\left(e_b + m_w h_0 a_s^2\right)\right]\right\},$$

Symbol	Value	Definition
a_0	5.43 Å	lattice constant of Si
a_S	7.68 Å	Step-edge lattice constant of (001)Si
h_0	1.38 Å	Monolayer step height of (001) $Ge_{0.4}Si_{0.6}$/Si
$e_{S_A,\,\mathrm{Si}}$	53 ± 26 meV	S_A step-edge energy of (001) Si
$e_{S_B,\,\mathrm{Si}}$	124 ± 27 meV	S_B step-edge energy of (001) Si
$e_{SNN,\,\mathrm{Si}}$	-67 ± 20 meV	Second nearest neighbor energy of (001) Si
$T_{R,\,\mathrm{Si}}$	1342 ± 108 K	Roughening temperature of (001) Si
$e_{S_A,\,\mathrm{Ge}}$	102 ± 7 meV	S_A step-edge energy of (001) Ge
$e_{S_B,\,\mathrm{Ge}}$	41 ± 7 meV	S_B step-edge energy of (001) Ge
$e_{SNN,\,\mathrm{Ge}}$	0 ± 5 meV	Second nearest neighbor energy of (001) Ge
$T_{R,\,\mathrm{Ge}}$	887 ± 115 K	Roughening temperature of (001) Ge
$e_{x(y)}$		step-edge energies in SOS model
e_b		unspecified bonding energy

Table 1. Physical Constants. Values for Si and Ge come respectively from

where a_s^2 is the area per lattice site. Using standard statistical mechanics techniques (Appendix A), the average film height is calculated as $\overline{h} = h_0 \langle H \rangle = \left(k_b T / a_s^2\right) \partial_{m_w} \ln Z = h_0 / \left\{ \exp\left[-\frac{1}{k_b T} \left(e_b + m_w h_0 a_s^2 \right) \right] - 1 \right\}$. Solving for m_w,

$$m_w = -\frac{1}{h_0 a_s^2} \left\{ k_b T \ln\left[1 + \left(h_0 / \overline{h} \right) \right] + e_b \right\}. \tag{10}$$

Plugging $m_w(\overline{h})$ back into Z, the wetting free energy density is found;

$$w_w\left(\overline{h}\right) = -\frac{k_b T}{a_s^2} \ln Z + m_w \overline{h} = \frac{k_b T}{a_s^2} \left\{ -\ln\left[1 + \left(\overline{h} / h_0 \right) \right] - \ln\left[1 + \left(h_0 / \overline{h} \right) \right] \left(h_0 / \overline{h} \right) \right\} - \frac{e_b \overline{h}}{a_s^2 h_0}.$$

Note that in the absence of fluctuations, $(T \to 0)$, $w_w(\overline{h}) \to -e_b \overline{h} / (h_0 a_s^2)$ as expected. It is easily verify that $m_w = \partial w_w / \partial \overline{h}$. The resulting wetting modulus is

$$w_w^{(2,0)} = \frac{\partial^2 w_w}{\partial \overline{h}^2} = \frac{k_b T}{a_s^2} \frac{1}{\overline{h}\left(h_0 + \overline{h} \right)}, \tag{11}$$

thus justifying the singular wetting potentials used in some modeling work. The bonding energy e_b is irrelevant to diffusive processes as it is constant and contributes nothing to the gradient of m_w or to the wetting modulus. If the bonding energy were a function of the film height (e.g. see Refs.[41,43]), then it would both complicate analysis and alter the form of the free energy and chemical potential. For example, one might hypothesize that the first layer has a lower bonding energy so that $e_b\left(h = h_0\right) = e_b - e_{\mathrm{interface}}$ and $e_b\left(h > h_0\right) = e_b$. This simple model demonstrates how even in the absence of any additional energy terms (*e.g.* see Ref.[43]), a thermodynamic wetting potential can develop merely due to the fact that the nearby film-substrate interface reduces configuration entropy by constraining height fluctuations.

3.2 Monte Carlo Simulations

Monte Carlo simulations[44] are used to calculate statistics of the full SOS model and subsequently to find the relationship between film-height $(\overline{h})$ and the wetting chemical potential (m_w) and the surface moduli ($w^{(2,0)}$, $w_x^{(2)}$, and $w_y^{(2)}$). In the SOS model, the energy of the surface is the total energy of the step edges,

$$u(h) = \sum_{\{i,j\}} e_x \left| h_{i,j} - h_{i+1,j} \right| + e_y \left| h_{i,j} - h_{i,j+1} \right|, \tag{12}$$

where h represents the set of all film heights over the entire lattice, $i = 1 \ldots N_x$, $j = 1 \ldots N_y$, and periodicity is assumed so that, $h_{-1,j} = h_{N_x,j}$, etc. This form issimilar to an Ising or Potts model. The binding energy (e_b) is neglected in these calculations because it does not effect diffusive processes and only shifts the chemical potential by a constant. Ideally, one

would like to calculate the partition function $Z = \sum_h \exp\{[-u(h) - m(\overline{h})h]/(k_bT)\}$, and the free energy, $f = -k_bT \ln Z + m(\overline{h})\overline{h}$ in terms of the order parameters $\overline{h}$ in full detail as in Sec. 3.1; however, one almost always settles for much less. Here, the average film-height is calculated for a given wetting chemical potential m_w, and the surface moduli of flat films are calculated.

3.2.1 Thermodynamic Quantities

The flat film configuration is translationally invariant, so the surface modulus can be expressed simply in Fourier space using the convention $h_{i,j} = \sum_{\mathbf{k}} e^{i\mathbf{k}\cdot\mathbf{x}_{i,j}} h_{\mathbf{k}}$ and $h_{\mathbf{k}} = (N_x N_y)^{-1} \sum_{\{i,j\}} e^{i\mathbf{k}\cdot\mathbf{x}_{i,j}} h_{i,j}$. In terms of the Fourier components, the partition function is

$$Z = \sum_h \exp\left\{ -\frac{1}{k_bT} \left[u(h) - A \sum_{\mathbf{k}} m_{-\mathbf{k}} h_{\mathbf{k}} \right] \right\} \tag{13}$$

where $A = N_x N_y a_s^2$.

For a flat film, all the chemical potential Fourier components are zero except for the $\mathbf{k} = 0$ component, $m_{\mathbf{k}\neq 0} = 0$ (Eq. 6). The $\mathbf{k} = \mathbf{0}$ component is $m_{\mathbf{0}} = m_w(\overline{h}_{\mathbf{0}})$, the wetting chemical potential of the flat film of height $\overline{h}_{\mathbf{0}}$, but the exact relationship between $m_{\mathbf{0}}$ and $\overline{h}_{\mathbf{0}}$ is not know *a priori*. The surface modulus (Eq. 5) is in general non-zero for all values of $\mathbf{k}$. Because of the symmetry of the simple square lattice, the tilt modulus has eigenvectors in the $x-$ and $y-$ directions, and thus has the form of Eq. 7. For each SOS Monte Carlo simulation, the wetting chemical potential m_w and temperature T are specified and the average film height ($\overline{h}_{\mathbf{0}}$), the wetting modulus ($w^{(2,0)}$), and tilt moduli ($w_x^{(2)}$ and $w_y^{(2)}$) are obtained.

The average film height is simple to obtain from each simulation; $\overline{h}_{\mathbf{0}} = \langle h_{\mathbf{0}} \rangle$. After a sufficient number of simulations with different m_w values, the relation can be inverted to give $m_{\mathbf{0}}(\overline{h}_{\mathbf{0}})$. The wetting and tilt moduli are more difficult. First, the film-height spectrum ($\langle |h_{\mathbf{k}}|^2 \rangle$) is obtained from the simulation (Fig. 3(b)). The surface modulus is related to the spectrum as (Appendix A)

$$w^{(2)}_{\mathbf{k},-\mathbf{k}} = \frac{k_bT}{A \left\langle |h_{\mathbf{k}}|^2 \right\rangle}. \tag{14}$$

The tilt moduli can be found by comparing $w^{(2)}_{\mathbf{k},-\mathbf{k}}$ to Eq. 7. There is a problem, though. The film-height gradient ($\nabla\overline{h}$) is only defined in the long wavelength limit, and Eq. 7 neglects high frequency roll-off due to the discrete lattice. Fortunately, simulated spectra appear to be consistent with a surface modulus of the form

$$w^{(2)}_{\mathbf{k},-\mathbf{k}} = w^{(2,0)} + a_s^{-2} \left[w_x^{(2)} \sin^2(a_s k_x) + w_y^{(2)} \sin^2(a_s k_y) \right]. \tag{15}$$

In the long wavelength limit, this form is equivalent to Eq. 7 , and it is also identical to the form one would obtain using a finite difference model of the free energy, i.e.

$$f \approx f_0 + a_s^2 w^{(1,0)} \sum_{\{i,j\}} \left(\overline{h}_{i,j} - \overline{h}_0\right) + \frac{1}{2} \sum_{\{i,j\}} \left[a_s^2 w^{(2,0)} \left(\overline{h}_{i,j} - \overline{h}_0\right)^2 + w_x^{(2)} \left(\overline{h}_{i,j} - \overline{h}_{i-1,j}\right)^2 + w_y^{(2)} \left(\overline{h}_{i,j} - \overline{h}_{i,j-1}\right)^2 \right].$$

Combining Eqs. 14 and 15, the surface moduli ($w^{(2,0)}$, $w_x^{(0,2)}$ and $w_y^{(0,2)}$) are obtained by fitting the theoretical surface height spectrum to the simulated spectrum using the fit function,

$$\left\langle |h_{\mathbf{k}}|^2 \right\rangle = k_bT \Big/ \left\{ A \left[w^{(2,0)} + w_x^{(2)} a_s^{-2} \sin^2(a_s k_x) + w_y^{(2)} a_s^{-2} \sin^2(a_s k_y) \right] \right\}.$$

3.2.2 Metropolis Algorithm

To find the various thermodynamic averages in Sec. 3.2.1, the Metropolis algorithm is used. This algorithm samples film height configurations in discrete steps. A particular configuration h will be sampled with a frequency proportional to its Gibbs factor, $GF = \exp\left\{ \left[-u(h) + \sum_{\{i,j\}} m_{i,j} h_{i,j} \right] / (k_bT) \right\}$. Film heights at individual lattice sites are randomly selected and then randomly raised or lowered. If the change raises, the Gibbs factor, it is accepted. If it lowers the Gibbs factor, it is accepted with a probability equal to the ratio of the Gibbs factors, $p_{\text{accept}} = GF_{\text{new}}/GF_{\text{old}}$. If a film height is proposed to be lower than zero, the step is rejected. Further details of the Metropolis algorithm can be found in one of the many treatments, for example Ref.[44]

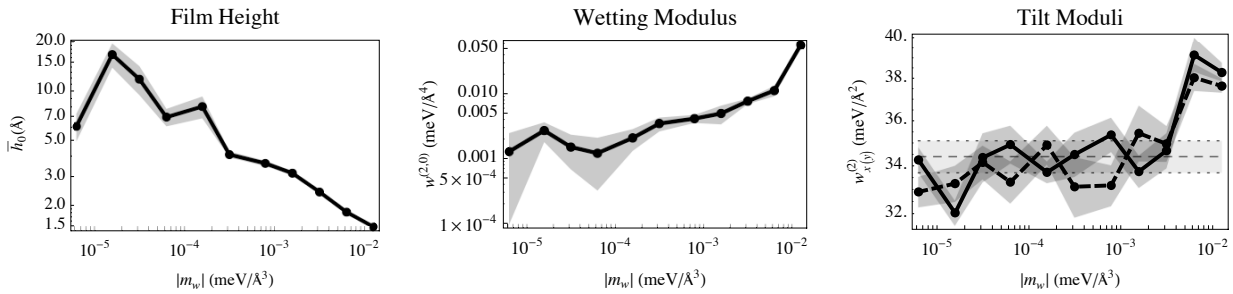

Figure 4. Film Height and Moduli vs. wetting chemical potential ($|m_w|$) from Monte Carlo Series 1 (Sec. 3.2.3). (a) Film height. (b) Wetting Modulus. (c) Tilt Moduli, where solid line is $w_x^{(2)}$, and dashed line is $w_y^{(2)}$. In all plots, gray shading indicates estimated statistical error in the Monte Carlo simulations. In (b) and (c), the thick film ($|m_w| = 0$) value is indicated for comparison as a horizontal dashed line with statistical simulation error shown in gray. In (c), only $w_x^{(2)}$ is shown for $|m_w| = 0$. $w_y^{(2)}$ is not shown, but close in value.

The Monte Carlo simulation is run for a around $10^5 N_x N_y$ steps, and statistics are gathered. Dimensionless variables are used: $H = \left[h_0^{-1}\right] h$, $H_{\mathbf{K}} = \left[h_0^{-1}\right] h_{\mathbf{k}}$, $\mathbf{X} = \left[a_s^{-1}\right] \mathbf{x}$, $\mathbf{K} = [a_s]\,\mathbf{k}$. The average film height ($\langle H_{\mathbf{0}} \rangle$) and spectrum ($\langle |H_{\mathbf{k}}|^2 \rangle$) are calculated by averaging over the entire simulation run. Every $10 N_x N_y$ Monte Carlo steps, the dimensionless film height and spectrum are recorded and the surface moduli are found using a least squares fit to a dimensionless version of Eq. 15. At the end of the simulation, the random errors in these numbers are estimated by guessing that the error is proportional to the square root of the number of steps.

3.2.3 Monte Carlo results

To keep the calculations as simple as possible, the second nearest neighbor interaction is neglected, $e_{SNN} = 0$, leaving four parameters that specify each simulation condition, the x- and y- step-edge energies, the wetting chemical potential, and the temperature $(e_x, e_y, |m_w|, T)$. m_w is always ≤ 0, so $|m_w|$ is reported. There are, however, only three parameters needed, as one can divide through by any parameter to obtain the exact same simulation, for example, $(1, e_y/e_x, |m_w|/e_x, T/e_x)$. Here, the full complement of four parameters is used to keep a clear link with the material system of interest, Ge_xSi_{1-x}/Si. To further simplify calculations, for most simulation series, an isotropic step-edge energy is used, that corresponds to e_{S_B} for $Ge_{0.34}Si_{0.66}/Si$, $e_x = e_y = e_{S_B} = 41.0$ meV. The corresponding predicted roughening temperature is $T_R = 539$ K. The simulation size is relatively small, $N_x = N_y = 32$, as opposed to $N_x = N_y = 512$, a typical value; however, significant results are obtained.

Three series of simulations were run:

1. First, a roughened isotropic film surface is studied with varying wetting chemical potential ($e_x = 41.0$ meV, $e_y = 41.0$ meV, $|m_w| = 0$ meV/Å^3 ... 12.58×10^{-3} meV/Å^3, $T = 595$ K). For the case of a thick film, $|m_w| = 0$ meV/Å^3, and $\overline{h}_{\mathbf{0}} \to \infty$, the resulting wetting modulus is $w^{(2,0)} = 1.3 \pm 1.0\left(10^{-3}\right)$ meV/Å^4, which is sufficiently close to zero, as expected. The tilt moduli are $w_x^{(2)} = 34.4 \pm 0.7$ meV/Å^2 and $w_y^{(2)} = 33.7 \pm 1.0$ meV/Å^2. $w_x^{(2)}$ and $w_y^{(2)}$ are expected to be equal since the step-edge energy is isotropic ($e_x = e_y$), and they are to within statistical error from the MC simulation. The corresponding dimensionless tilt moduli are $W_x^{(2)} = [h_0^2/(k_b T)] w_x^{(2)} = 1.28 \pm 0.03$ and $W_y^{(2)} = [h_0^2/(k_b T)] w_y^{(2)} = 1.25 \pm 0.04$ which are fairly close to unity; thus, $k_b T/h_0^2$ appears to be a reasonable order of magnitude estimate of the tilt modulus near the roughening temperature. Fig. 4 shows the film height and other moduli for other values of the wetting chemical potential. As $|m_w|$ increases, the film height decreases, and the wetting modulus and tilt moduli increase. Within statistical error, the $x-$ and $y-$ tilt moduli remain equal as expected. The low film height for $|m_w| = 6.29 \times 10^{-6}$ meV/Å^3 is probably a statistical anomaly. For such small wetting chemical potentials, the film heights fluctuate quite a bit. This data point should be checked with longer runs and larger simulations.

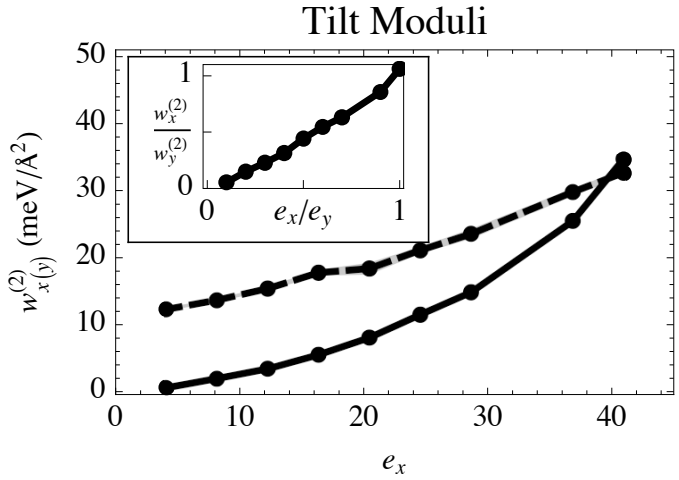

Figure 5. Tilt Moduli of anisotropic thick film surfaces as a function of e_x for simulation series 2 (Sec. 3.2.3). Solid line shows $w_x^{(2)}$. Dashed line shows $w_y^{(2)}$. The inset shows the tilt moduli ratio ($w_x^{(2)}/w_y^{(2)}$) as function of the step-edge energy ratio (e_x/e_y).

2. Next, a thin faceted film ($T < T_R$) is studied ($e_x = 41.0$ meV, $e_y = 41.0$ meV, $|m_w| = 252 \times 10^{-6}$ meV/Å^3, $T = 476$ K). The mean film height was $\bar{h}_{\mathbf{0}} = 2.76$ Å which is equal to the simulation starting value prior to the equilibration period. The faceted film cannot fluctuate enough to change its mean height. Consequently, it never finds it's true equilibrium value. The resulting wetting and tilt moduli are $w^{(2,0)} = 1.03 \pm 0.01$ meV/Å^4, $w_x^{(2)} = 62.3 \pm 0.3$ meV/Å^2 and $w_y^{(2)} = 62.2 \pm 0.3$ meV/Å^2. Note that the tilt moduli are about a factor of two greater than the tilt moduli found for the roughened films. Moreover, the wetting modulus is enormous, about 10^3 times that of a similar roughened film, and form that 10^5 times larger than the ratio $|m_w|/h_0$ which has the same dimensions and should have the same order of magnitude. This discrepancy is due to the fact that the wetting energy $w_w(\bar{h})$ is not a monotonically varying function for a faceted film. Huse[45] suggested that it is a corrugated potential, $w_w\left(\bar{h}\right) \approx A\bar{h}^{-n} + B\cos(2\pi\bar{h}/h_0)$. Thus, the wetting modulus $w^{(2,0)}$ is essentially measuring the curvature of the $w_w\left(\bar{h}\right)$ near the minimum of an oscillation. It is also interesting to note that the surface modulus is not infinite as suggested by Eqs. 1 and 2. This discrepancy is due to the fact that Eqs. 1 and 2 are asymptotic approximations appropriate to large slopes ($\nabla\bar{h}$), while the expansion in the surface energy (Eq. 4) is applicable to the case of small slopes. This last point would be merely academic, except that it raises the question of what happens during partial monolayer coverage. For example, at $\bar{h}_{\mathbf{0}} = 2.5h_0$, the oscillating wetting energy would be a maximum, leading to a negative surface modulus. The film surface would then be hypersuceptible to an instability such as the ATG instability. At slightly greater than $\bar{h}_{\mathbf{0}} = 2.25h_0$, the wetting modulus should vanish. Can this fact be used to predict a transition from stable 2D growth to unstable 3D growth for some film height corresponding to near 25% coverage, $\bar{h}_{\mathbf{0}} = (n + 0.25)h_0$? If so, this would be essentially a fourth mechanism, an ATG instability for faceted crystal surfaces.

3. Finally, a roughened anisotropic thick film surface is studied with varying x-step-edge energy, e_x ($e_x = 4.10$ meV$\ldots 41.0$ meV, $e_y = 41.0$ meV, $|m_w| = 0$ meV/Å^3, $T = 595$ K). The ratio of e_x/e_y varies from $0.1\ldots 1$. For the roughened thick film, the wetting modulus is zero. Fig. 5 shows the resulting tilt moduli and their ratios. The lower value of e_x has two effects. First, it changes the ratio of the tilt moduli. Although not exact, $w_x^{(2)}/w_y^{(2)} \sim e_x/e_y$. Second, it lowers the value of both tilt moduli. It is obvious that x-tilt modulus should be lower when e_x is decreased, but the y-tilt modulus is lower because steps in the y-direction have a lower free energy due to the greater ease of producing kinks whose energy is proportional to e_x.

4. CONCLUSIONS

Three different models of the free energy of a (001) crystal surface I. faceted, II. thermally roughened, and III. antifaceted give rise to three different epitaxial self-assembled quantum dot (SAQD) growth mechanisms, respectively, I. nucleation and growth, II. Asarro-Tiller-Grinfeld (ATG) instability and III. non-linear instability. The distinction between these models depends on the energy and free energy of strained step-edges on the (001) surface. A simplified strain-dependent free

energy model for monolayer steps in Ge_xSi_{1-x}/Si surfaces was developed that was based on prior modeling that indicated that these step-edges have strain-dependent energies[23] and a step-edge free energy model.[39,40] Although very approximate, this step-edge free energy model yielded a phase diagram in the composition (x) – temperature (T) plane that has four regions, three of which correspond to the three SAQD growth mechanisms (I-III), with the status of region III remaining somewhat ambiguous. The fourth is simply the freeze-out region where diffusion is extremely slow. For a selected value of the step-edge strain sensitivity, strong agreement with experimental observations of Ge_xSi_{1-x}/Si growth[20] was observed. Based on these findings, a simplified Solid-On-Solid (SOS) model was applied to the case of thermally roughened surfaces (II) to calculate the surface moduli (resistance to deformation) from the step-edge energy. An entropic contribution to the wetting potential was identified, and the tilt-moduli that are related to the surface free energy density were calculated. Additionally, a possible fourth mechanism was proposed where a faceted surface with an incomplete monolayer might be susceptible to the ATG instability. Finally, the effects of step-edge energy anisotropy were investigated, and it was found that the tilt moduli show an anisotropy that is nearly proportional to the step-edge energy anisotropy, a finding with applications to III-V or II-VI semiconductor films such as $In_xGa_{1-x}As/GaAs$.

The models presented here were constructed to be as simple as possible and still generate qualitatively correct and quantitatively reasonable results. Additionally, there was a great deal of statistical error and possibly error from small simulation size. It will be worthwhile to increase the simulation size and run for longer times, but only after more sophisticated simulations corresponding to the diamond or zinc-blend structure are developed. It might also be important to incorporate surface tension effects directly.[46] Despite these limitations, the findings from these simple small models are clear, they help to clarify a situation that has been ambiguous for some time, and they will form the foundation of a more rigorous modeling effort.

APPENDIX A. STANDARD STATISTICAL MECHANICS RELATIONS

Start from a general partition function obtained from multiple complex configurational variables ($h = \{h_i\}$) and general complex chemical potentials $m = \{m_i\}$,

$$Z = \sum_h \exp\left[-\frac{1}{k_bT}\left(u(h) - a\sum_i (m_i^* h_i + m_i h_i^*)\right)\right].$$

a is a constant, and $\sum_h$ indicates a sum over all possible values of the variables, $\{h_i\}$. From this partition function, the following relations can be derived, and they are used in Sec. 3:

$$\overline{h}_i = \langle h_i \rangle = \frac{k_bT}{a}\frac{\partial \ln Z}{\partial m_i^*}.$$

$$f = -k_bT \ln Z + a\sum_i \left(m_i^* \overline{h}_i + m_i \overline{h}_i^*\right).$$

$$\frac{1}{a}\frac{\partial f}{\partial \overline{h}_i^*} = m_i.$$

$$\frac{1}{a}\frac{\partial^2 f}{\partial \overline{h}_j \partial \overline{h}_i^*} = \frac{\partial m_i}{\partial \overline{h}_j} = \frac{k_bT}{a}\left[\langle h_i^* h_j \rangle - \overline{h}_i^* \overline{h}_j\right]^{-1},$$

where $[\,]^{-1}$ should be interpreted as the matrix inversion. When h_i and h_j are Fourier components, $i = \mathbf{k}_1$, and $j = \mathbf{k}_2$, and $\overline{h}_i = \overline{h}_j = 0$, one can use translational symmetry to show that

$$\frac{1}{a}\frac{\partial^2 f}{\partial \overline{h}_{\mathbf{k}_2} \partial \overline{h}_{\mathbf{k}_1}^*} = \frac{k_bT\,\delta_{\mathbf{k}_1 - \mathbf{k}_2}}{a\left\langle |h_{\mathbf{k}_1}|^2 \right\rangle}.$$

REFERENCES

[1] Li, S.-S., Xia, J.-B., Yuan, Z. L., Xu, Z. Y., Ge, W., Wang, X. R., Wang, Y., Wang, J., and Chang, L. L., "Effective-mass theory for InAs/GaAs strained coupled quantum dots," *Phys. Rev. B* **54**, 11575–11581 (Oct 1996).

[2] Li, S.-S. and Xia, J.-B., "Intraband optical absorption in semiconductor coupled quantum dots," *Phys. Rev. B* **55**, 15434–15437 (Jun 1997).

[3] Bimberg, D., Grundmann, M., and Ledentsov, N. N., [*Quantum Dot Heterostructures*], John Wiley & Sons (1999).

[4] Pchelyakov, O. P., Bolkhovityanov, Y. B., Dvurechenski, A. V., Sokolov, L. V., Nikiforov, A. I., Yakimov, A. I., and Voigtländer, B., "SiliconGermanium nanostructures with quantum dots: Formation mechanisms and electrical properties," *Semiconductors* **34**(11), 122947 (2000). [doi:10.1134/1.1325416].

[5] Grundmann, M., "The present status of quantum dot lasers," *Physica E* **5**, 167 (2000). [doi:10.1016/S1386-9477(99)00041-7].

[6] Petroff, P. M., Lorke, A., and Imamoglu, A., "Epitaxially self-assembled quantum dots," *Physics Today* , 46–52 (May 2001). [doi:10.1063/1.1381102].

[7] Liu, H.-Y., Xu, B., Wei, Y.-Q., Ding, D., Qian, J.-J., Han, Q., Liang, J.-B., and Wang, Z.-G., "High-power and long-lifetime InAs/GaAs quantum-dot laser at 1080 nm," *Applied Physics Letters* **79**(18), 2868–70 (2001). [doi:10.1063/1.1415416].

[8] Bimberg, D., Ledentsov, N., and Lott, J., "Quantum-dot vertical-cavity surface-emitting laser," *MRS Bulletin* **27**(7), 531–7 (2002).

[9] Friesen, M., Rugheimer, P., Savage, D. E., Lagally, M. G., van der Weide, D. W., Joynt, R., and Eriksson, M. A., "Practical design and simulation of silicon-based quantum-dot qubits," *Physical Review B* **67**(12), 121301 (R) (2003). [doi:10.1103/PhysRevB.67.121301].

[10] Cheng, Y.-C., Yang, S., Yang, J.-N., Chang, L.-B., and Hsieh, L.-Z., "Fabrication of a far-infrared photodetector based on InAs/GaAs quantum-dot superlattices," *Optical Engineering* **42**(1), 11923 (2003). [doi:10.1117/1.1525277].

[11] Sakaki, H., "Progress and prospects of advanced quantum nanostructures and roles of molecular beam epitaxy," *Journal of Crystal Growth* **251**, 9–16 (2003). [doi:10.1016/S0022-0248(03)00831-5].

[12] Spencer, B. J., Voorhees, P. W., and Davis, S. H., "Morphological instability in epitaxially strained dislocation-free films," *Physical Review Letters* **67**(26), 3696–3699 (1991). [doi:10.1103/PhysRevLett.67.3696].

[13] Brunner, K., "Si/ge nanostructures," *Reports on Progress in Physics* **65**(1), 27–72 (2002). [doi:10.1088/0034-4885/65/1/202].

[14] Freund, L. B. and Suresh, S., [*Thin Film Materials: Stress, Defect Formation and Surface Evolution*], ch. 8, Cambridge University Press (2003).

[15] Tersoff, J. and LeGoues, F. K., "Competing relaxation mechanisms in strained layers," *Physical Review Letters* **72**, 3570–3573 (May 1994). [doi:10.1103/PhysRevLett.72.3570].

[16] Asaro, R. and Tiller, W., "Interface morphology development during stress corrosion cracking: Part i. via surface diffusion," *Metallurgical and Materials Transactions B* **3**(7), 1789–1796 (1972).

[17] Grinfeld, M. A., "Instability of the separation boundary between a non-hydrostatically stressed elastic body and a melt.," *Soviet Physics Doklady* **31**, 831–4 (1986).

[18] Srolovitz, D. J., "On the stability of surfaces of stressed solids," *Acta Metallurgica* **37**(2), 621–625 (1989). [doi:10.1016/0001-6160(89)90246-0].

[19] Shenoy, V. B. and Freund, L. B., "A continuum description of the energetics and evolution of stepped surfaces in strained nanostructures," *Journal of the Mechanics and Physics of Solids* **50**(9), 1817–1841 (2002).

[20] Tromp, R. M., Ross, F. M., and Reuter, M. C., "Instability-driven sige island growth," *Phys. Rev. Lett.* **84**, 4641–4644 (May 2000).

[21] Vailionis, A., Cho, B., Glass, G., Desjardins, P., Cahill, D. G., and Greene, J. E., "Pathway for the strain-driven two-dimensional to three-dimensional transition during growth of ge on si(001)," *Phys. Rev. Lett.* **85**, 3672–3675 (Oct 2000).

[22] Tersoff, J., Spencer, B. J., Rastelli, A., and von Känel, H., "Barrierless formation and faceting of SiGe islands on Si(001)," *Phys. Rev. Lett.* **89**, 196104 (Oct 2002).

[23] Shenoy, V. B., Ciobanu, C. V., and Freund, L. B., "Strain induced stabilization of stepped Si and Ge surfaces near (001)," *Applied Physics Letters* **81**(2), 364–366 (2002).

[24] Friedman, L. H., "Anisotropy and morphology of strained III-V heteroepitaxial films," *Physical Review B (Condensed Matter and Materials Physics)* **78**(19), 193302 (2008).

[25] Friedman, L. H., "Stochastic continuum modeling self-assembled epitaxial quantum dot formation," *Nanostructured Thin Films* **7041**(1), 704103, SPIE (2008).

[26] Zhang, Y., Bower, A., and Liu, P., "Morphological evolution driven by strain induced surface diffusion," *Thin solid films* **424**, 9–14 (2003). [doi:10.1016/S0040-6090(02)00897-0].

[27] Friedman, L., "Predicting and understanding order of heteroepitaxial quantum dots," *Journal of Electronic Materials* **36**(12), 1546–1554 (2007).

[28] Lee, H., Yang, W., Sercel, P., and Norman, A., "The shape of self-assembled InAs islands grown by molecular beam epitaxy," *Journal of Electronic Materials* **28**(5), 481–485 (1999).

[29] Jeong, H.-C. and Williams, E. D., "Steps on surfaces: experiment and theory," *Surface Science Reports* **34**(6-8), 171–294 (1999).

[30] Cross, M. C. and Hohenberg, P. C., "Pattern formation outside equilibrium," *Reviews of Modern Physics* **65**(3), 851–1112 (1993). [doi:10.1103/RevModPhys.65.851].

[31] Golovin, A. A., Davis, S. H., and Voorhees, P. W., "Self-organization of quantum dots in epitaxially strained solid films," *Physical Review E* **68**, 056203 (2003). [doi:10.1103/PhysRevE.68.056203].

[32] Golovin, A. A., Levine, M. S., Savina, T. V., and Davis, S. H., "Faceting instability in the presence of wetting interactions: A mechanism for the formation of quantum dots," *Physical Review B* **70**, 235342 (2004). [doi:10.1103/PhysRevB.70.235342].

[33] Obayashi, Y. and Shintani, K., "Directional dependence of surface morphological stability of heteroepitaxial layers," *Journal of Applied Physics* **84**(6), 3141 (1998). [doi:10.1063/1.368468].

[34] Ozkan, C. S., Nix, W. D., and Gao, H. J., "Stress-driven surface evolution in heteroepitaxial thin films: Anisotropy of the two-dimensional roughening mode," *JOURNAL OF MATERIALS RESEARCH* **14**, 3247–3256 (Aug 1999). [doi:10.1557/JMR.1999.043].

[35] Ramasubramaniam, A. and Shenoy, V. B., "Three-dimensional simulations of self-assembly of hut-shaped Si-Ge quantum dots," *Journal of Applied Physics* **95**, 7813–7824 (Jun 2004).

[36] Chokshi, N. S. and Millunchick, J. M., "Cooperative nucleation leading to ripple formation in InGaAs/GaAs films," *Applied Physics Letters* **76**(17), 2382–2384 (2000).

[37] Liang, B. L., Wang, Z. M., Mazur, Y. I., Strelchuck, V. V., Holmes, K., Lee, J. H., and Salamo, G. J., "InGaAs quantum dots grown on B-type high index GaAs substrates: surface morphologies and optical properties," *Nanotechnology* **17**(11), 2736–2740 (2006). [doi:10.1088/0957-4484/17/11/004].

[38] Schmidbauer, M., Seydmohamadi, S., Grigoriev, D., Wang, Z. M., Mazur, Y. I., Schafer, P., Hanke, M., Kohler, R., and Salamo, G. J., "Controlling planar and vertical ordering in three-dimensional (In,Ga)As quantum dot lattices by GaAs surface orientation," *Phys. Rev. Lett.* **96**, 066108 (Feb 2006).

[39] Zandvliet, H. J. W., "Energetics of Si(001)," *Rev. Mod. Phys.* **72**, 593–602 (Apr 2000).

[40] Zandvliet, H. J. W., "Determination of Ge(001) step free energies," *Phys. Rev. B* **61**, 9972–9974 (Apr 2000).

[41] Prasad, A. and Weichman, P. B., "Layering transitions, disordered flat phases, reconstruction, and roughening," *Phys. Rev. B* **57**, 4900–4938 (Feb 1998).

[42] Swendsen, R. H., "Monte carlo studies of the interface roughening transition," *Phys. Rev. B* **15**, 5421–5431 (Jun 1977).

[43] Beck, M. J., van de Walle, A., and Asta, M., "Surface energetics and structure of the Ge wetting layer on Si(100)," *Physical Review B* **70**, 205337 (Nov 2004). [doi:10.1103/PhysRevB.70.205337].

[44] Newman, M. E. J. and Barkema, G. T., [*Monte Carlo Methods in Statistical Physics*], Oxford University Press (1999).

[45] Huse, D. A., "Renormalization-group analysis of layering transitions in solid films," *Phys. Rev. B* **30**, 1371–1376 (Aug 1984).

[46] Gutheim, F., Müller-Krumbhaar, H., Brener, E., and Kaganer, V., "Thermal roughening of a solid-on-solid model with elastic interaction," *Phys. Rev. B* **67**, 195404 (May 2003).